Processes Contributing to North American Cold Air Outbreaks Based on Air Parcel Trajectory Analysis

KARA HARTIG[a], ELI TZIPERMAN,[b,c] AND CHRISTOPHER P. LOUGHNER[d]

[a] *Department of Physics, Harvard University, Cambridge, Massachusetts*
[b] *Department of Earth and Planetary Sciences, Harvard University, Cambridge, Massachusetts*
[c] *School of Engineering and Applied Sciences, Harvard University, Cambridge, Massachusetts*
[d] *NOAA/Air Resources Laboratory, College Park, Maryland*

ABSTRACT: Wintertime cold air outbreaks are periods of extreme cold, often persisting for several days and spanning hundreds of kilometers or more. They are commonly associated with intrusions of cold polar air into the midlatitudes, but it is unclear whether the air mass's initial temperature in the Arctic or its cooling as it travels is the determining factor in producing a cold air outbreak. By calculating air parcel trajectories for a preindustrial climate model scenario, we study the role of the origin and evolution of air masses traveling over sea ice and land and resulting in wintertime cold air outbreaks over central North America. We find that not all Arctic air masses result in a cold air outbreak when advected into the midlatitudes. We compare trajectories that originate in the Arctic and result in cold air outbreaks to those that also originate in the Arctic but lead to median temperatures when advected into the midlatitudes. While about one-third of the midlatitude temperature difference can be accounted for by the initial height and temperature in the Arctic, the other two-thirds are a result of differences in diabatic heating and cooling as the air masses travel. Vertical mixing of cold surface air into the air mass while it travels dominates the diabatic cooling and contributes to the cold events. Air masses leading to cold air outbreaks experience more negative sensible heat flux from the underlying surface, suggesting that preconditioning to establish a cold surface is key to producing cold air outbreaks.

SIGNIFICANCE STATEMENT: Wintertime cold air outbreaks can cause temperatures to plummet tens of degrees below freezing over the northern United States, with the potential to damage agriculture, infrastructure, and human health. Accurate predictions under climate change could help mitigate these effects, but there is disagreement over whether cold air outbreaks have declined in line with the already-observed global warming trend or persisted in spite of it. Focusing on cold air outbreaks that originate from the Arctic, we find that there must be additional cooling of the traveling air mass by mixing with very cold surface air as it moves south over North America in order to result in a cold outbreak.

KEYWORDS: Arctic; North America; Lagrangian circulation/transport; Trajectories; Cold air surges; Diabatic heating

1. Introduction

Wintertime cold air outbreaks (CAO) occur when surface temperatures drop well below the climatological average. They are most commonly defined as large-scale periods of extreme cold persisting for several days and are often associated with intrusions of cold polar air into the midlatitudes (Walsh et al. 2001; Cellitti et al. 2006; Portis et al. 2006; Vavrus et al. 2006; Kolstad et al. 2010; Hankes and Walsh 2011; Smith and Sheridan 2018). These cold air outbreaks are often associated with the negative phase of the Northern Annular Mode/North Atlantic Oscillation (Thompson and Wallace 2001; Hurrell et al. 2003; Cellitti et al. 2006), which can be influenced by sudden stratospheric warmings (Gerber et al. 2012; Hitchcock and Simpson 2014; Kidston et al. 2015). Over the ocean, cold air outbreaks can influence the extent of sea ice and the strength of ocean circulations through bursts of strong air–sea heat exchange (Kolstad et al. 2010; Papritz et al. 2015; Papritz

and Spengler 2017). Over land, their effects on humans are more direct, as cold air outbreaks can damage agriculture and infrastructure, put additional strain on energy systems, and increase mortality (Quiroz 1984; Rogers and Rohli 1991; Smith and Sheridan 2019). The largest impacts tend to occur in areas where cold air outbreaks are rare (Smith and Sheridan 2019). As a result, understanding the drivers of variability over space and time and predicting how they will evolve, particularly in the context of climate change, is key to improving forecasts and preparedness.

In spite of a clear warming trend in the global average temperature over the past several decades (Arias et al. 2021), there is disagreement over whether a similar warming trend has occurred in cold air outbreaks. Some studies have observed a decrease in frequency, duration, and intensity of cold air outbreaks over the last few decades (Hankes and Walsh 2011; Robeson et al. 2014; Screen 2014; van Oldenborgh et al. 2019; Smith and Sheridan 2020), following the trend in global average temperature. However, warm and cold extremes do not necessarily track the mean response. Other studies have detected no trend in cold air outbreaks (Walsh et al. 2001; Portis

---

Corresponding author: Kara Hartig, kara_hartig@g.harvard.edu

et al. 2006; Westby et al. 2013) or even a slight increase in recent decades (Liu et al. 2012; Cohen et al. 2014), indicating that some mechanism may be acting to maintain cold extremes in spite of the robust increase in average temperature. This lack of consensus in observed trends highlights the need to understand the mechanisms influencing cold air outbreaks if we are to make reliable predictions.

Predicting the response of cold air outbreaks to future warming must rely in large part on climate models, and while most show a decline in cold air outbreaks by the end of the century, the regional and near-term response is much more variable. By the end of the century, there is near-universal agreement across models that the global warming signal will begin to dominate regional variability and cold air outbreaks will decrease everywhere in a "business-as-usual" emissions scenario (Vavrus et al. 2006; Gao et al. 2015). Regional variations will remain significant, as there are indications that regions with a historically high occurrence will see a smaller decline in cold air outbreaks (Gao et al. 2015), but all regions are expected to see some decline by the year 2100. However, near-term trends are much more variable. In some models, there are regions with no trend or even a slight increase in cold air outbreaks by midcentury (Vavrus et al. 2006), indicating that many regions will continue to experience extreme cold air outbreaks for decades to come.

Three main approaches have emerged to study the mechanisms leading to cold air outbreaks, which we build upon in this work. Idealized column models have demonstrated the importance of radiative cooling, and particularly its enhancement or suppression by liquid and ice condensates, in the formation of cold continental air, but are unable to represent mixing with surrounding air masses (Curry 1983; Cronin and Tziperman 2015). Another approach is based on an Eulerian breakdown of advection and other contributions to the temperature budget in regions upwind of cold air outbreaks. This Eulerian approach has identified the main processes affecting cold air outbreaks to be horizontal advection, adiabatic heating through subsidence, and diabatic processes (Konrad and Colucci 1989; Portis et al. 2006; Screen 2014; Wang et al. 2019). Such studies typically presupposed a particular path of travel for cold air outbreaks and combined all diabatic processes into a single term, which did not allow them to pick out specific physical mechanisms responsible for the cold events.

Another approach uses Lagrangian trajectories of air masses resulting in cold air outbreaks to track temperature changes for individual air parcels in realistic flows over topography and changing surfaces. However, such studies typically used the change in potential temperature along the trajectory to deduce the total diabatic heating and were therefore also unable to attribute the temperature change to specific physical mechanisms beyond, at best, surface fluxes and latent heating (Papritz et al. 2015; Papritz and Spengler 2017; Hermann et al. 2020). Using the trajectory approach, Walsh et al. (2001) found that cold air outbreaks over continental North America generally travel southward and southeastward, carrying cold polar air out of the Arctic and into the midlatitudes. Subsequent studies have identified the Arctic Ocean and northern Canada as important origin regions for cold air outbreaks, postulating that changes

in temperature there will directly affect the intensity of cold air outbreaks downstream (Konrad and Colucci 1989; Kalkstein et al. 1990; Hankes and Walsh 2011).

But origin alone may not determine a cold air outbreak, as adiabatic and diabatic effects can also act to alter the temperature of an air mass as it travels. Curry (1983) identified radiative cooling, particularly by liquid and ice condensates, as a key contributor to cold air formation using a column model. Cronin and Tziperman (2015) found that in a warmer climate, moist warm air coming from the ocean can lead to the formation of low clouds; the greenhouse effect of these clouds prevents the formation of polar air masses and can dramatically reduce the occurrence of cold events. André and Mahrt (1982) found that both radiative cooling and upward mixing of cold surface air are important in the formation of cold air masses near the surface by analyzing radiosonde data of the wintertime surface temperature inversion over land.

Our approach goes one step further, calculating Lagrangian trajectories and breaking down the diabatic heating term into contributions from radiation, latent heating, and turbulent mixing to determine the physical mechanisms leading to cold air outbreaks. Our objective is to examine the relative importance of origin versus diabatic evolution of air masses traveling over sea ice and land, which result in midlatitude cold air outbreaks over North America. To focus on natural variability and avoid possible complicating factors due to a climate change signal, we perform our analysis on a control run of a prescribed SST atmospheric model run at fixed preindustrial CO_2 concentration. We identify cold air outbreaks over the interior of North America, calculate 10-day back trajectories for each, and analyze both the initial temperature and the temperature tendencies due to different physical processes along those trajectories. These trajectories are then compared to those of air masses that follow a similar path out of the Arctic but result in median temperatures on arrival in the midlatitudes to isolate the characteristics that cause Arctic air masses to become cold air outbreaks. With this approach, we seek to address the following questions:

- To what extent does initial temperature versus diabatic evolution determine whether an Arctic air mass becomes a cold air outbreak?
- Which diabatic processes have the greatest contribution to cold airmass development, and what characteristics of the surface and atmosphere favor them?

Section 2 (methods) describes the climate model, identification of cold air outbreaks and median-temperature events (MTE), trajectory calculation, and selection of trajectories for analysis. Section 3 (results) details our main findings: not all Arctic air masses advected into the midlatitudes result in cold air outbreaks. That is, low initial temperatures in the origin region alone do not necessarily lead to a cold air outbreak. Both longwave radiation and vertical mixing result in significant temperature change along trajectories. We find that trajectories leading to cold air events are more strongly affected by vertical mixing than similar trajectories that lead to median-temperature events. Cold air outbreaks experience more
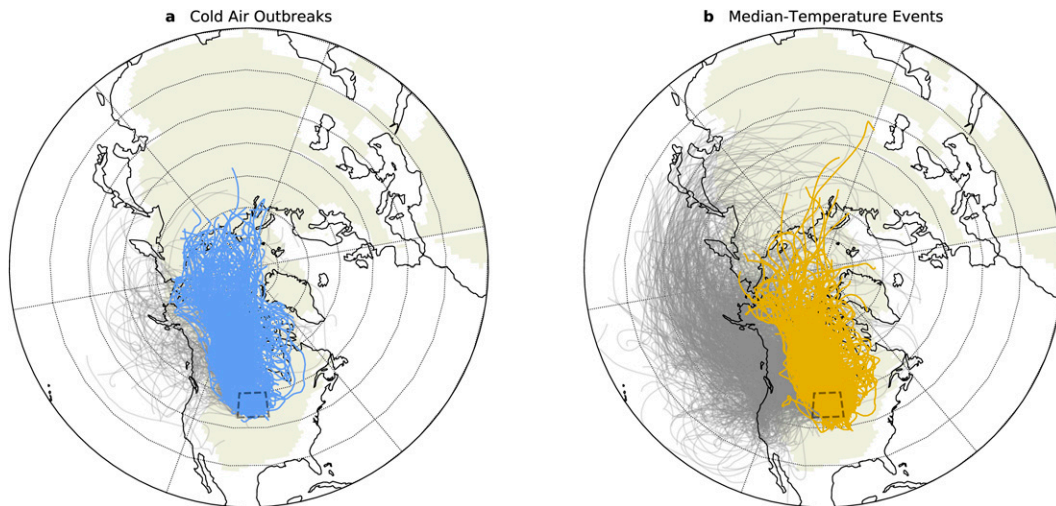
FIG. 1. Trajectories arriving in the study region (black dashed box) over North America. Each line represents a 10-day back trajectory for events drawn from the (a) coldest 5% and the (b) median 10% of the temperature anomaly distribution in the study region over 51 winters of preindustrial CESM data. Gray lines show trajectory paths for all 400 cold air outbreaks in (a) and 1000 median-temperature events in (b). The shaded beige region is a mask (see section 2 for a description) used to select for the trajectories coming out of the Arctic analyzed in this study; trajectories that never leave the mask are shown in blue for cold air outbreaks (the CAO sample) in (a) and in gold for median-temperature events (the MTE sample) in (b).

negative sensible heat flux from the underlying surface and are accompanied by lower net solar flux at the surface, indicating that conditions favorable to cold air outbreaks include the establishment of a cold surface.

2. Methods

We use climate model output from CESM1.2 (Hurrell et al. 2013) with CAM5 (Neale et al. 2012) to study cold air outbreaks. We use a preindustrial climate scenario, with CO_2 and other constituents fixed at 1850 levels, along with prescribed sea surface temperatures and sea ice at $0.9° \times 1.25°$ resolution with 30 vertical levels (component set F_1850_CAM5 with resolution f09_f09). The model was run for 56 years with the first few years discarded to allow for spin-up, resulting in 51 complete winters of data. Previous studies using Lagrangian air parcel tracking generally use the ERA-Interim product (Bieli et al. 2015; Papritz et al. 2015; Papritz and Spengler 2017; Zschenderlein et al. 2019; Hermann et al. 2020), which has a higher vertical resolution near the surface than our CAM configuration (Dee et al. 2011). However, the model diagnostics that enable us to break down the temperature change into distinct physical processes are not readily available in reanalysis products, so we elected to use CAM with much higher temporal output frequency (every hour rather than the typical 6 h) instead.

To investigate cold air outbreaks in this model, we began by defining a sampling region 12° longitude × 7° latitude in the interior of North America (the black dashed box in Fig. 1; 43°–50°N, 92°–104°W). The sampling region was selected to overlap with a region of high cold air outbreak occurrence (Walsh et al. 2001; Westby et al. 2013; Gao et al. 2015) while

remaining far enough from the Rocky Mountains to avoid direct topographic effects for simplicity and small enough that it is reasonable to average across distinct trajectories. Within the sampling region, we calculated the winter surface temperature anomaly as the hourly 2-m temperature minus the DJF seasonal mean at each grid point, then sorted all temperature anomalies from smallest to largest to construct a temperature anomaly distribution. From this distribution, we drew 400 samples from the coldest 5% and another 1000 samples from the median 10%, each sample at least 3 days apart from every other sample, providing candidates for both cold air outbreaks and median-temperature events.

From each event sample, representing a position in time, latitude, and longitude, we calculated a 10-day back trajectory. The back trajectory calculations were performed using HYSPLIT, a trajectory and dispersion calculation tool developed by NOAA's Air Resources Laboratory (Draxler and Hess 1998, 1997; Draxler 1999; Stein et al. 2015). We found that trajectories out of the Arctic, such as those used in this study, travel through sharp vertical temperature inversions and are frequently close to the topography, so it is particularly important to accurately estimate the precise vertical position within the inversion and height above the surface. To increase the accuracy of the trajectories, we therefore improved the precision of the input meteorological data [by adding variables that are the difference between the original (uncompressed) and the packed (compressed) data and improve data precision within HYSPLIT, for winds, temperature, and humidity (DIFF; NOAA/ARL 2022)] and doubled the vertical resolution of HYSPLIT's internal sigma levels onto which the meteorological data are interpolated. For each cold air outbreak or median-temperature candidate identified above, we
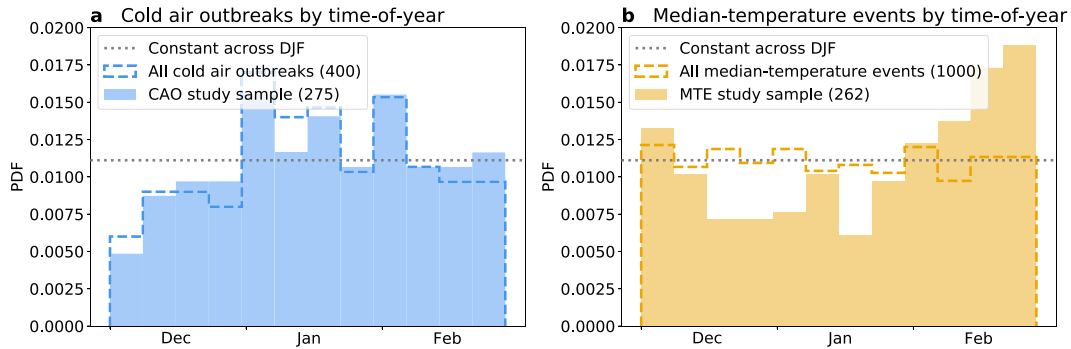
FIG. 2. Probability distribution function of events sampled within the DJF winter season is shown for (a) all sampled cold air outbreaks (400 events; blue dashed outline) and the corresponding study sample CAO (275 events; blue solid bars) and for (b) all sampled median-temperature events (1000 events; gold dashed outline) and the corresponding study sample MTE (262 events; gold solid bars). The horizontal black dotted line represents the probability density expected if events were equally likely to occur across all of DJF.

initialized a 10-day backward trajectory starting 100 m above ground level at the grid point corresponding to the sampled temperature anomaly, resulting in 400 cold air and 1000 median-temperature trajectories.

We found that while cold air outbreak candidates generally travel out of the Arctic and southeastward over North America toward our sampling region (gray lines in Fig. 1a), median-temperature candidate trajectories have a wider spread, often passing over the Pacific (gray lines in Fig. 1b). To isolate the mechanisms that determine whether an Arctic air mass becomes a midlatitude cold air outbreak, we want to compare cold air outbreak trajectories to median-temperature trajectories that follow a similar path out of the Arctic but do not result in cold air outbreaks. To this end, we constructed a mask (beige regions in Fig. 1) by combining all Northern Hemisphere grid points with a land fraction greater than 80% or a DJF-averaged sea ice fraction greater than 10%. We shrank the mask an additional 7° longitude away from all coasts, then selected only those trajectories that remained on the mask (i.e., stayed over land or sea ice) for all 10 days. The on-mask trajectories, CAO (275 trajectories) and MTE (262 trajectories), form the study sample used throughout the analysis that follows and are shown in blue for CAO and gold for MTE in Fig. 1.

Meteorological variables were traced along each trajectory offline by interpolating data output by CESM directly onto those trajectory positions. The trajectories output by HYSPLIT list the latitude, longitude, and pressure of the air parcel every hour. For a given trajectory, the interpolation of meteorological variables was done point by point, first interpolating the variable in time, latitude, and longitude onto the trajectory position, converting from CAM's hybrid sigma-pressure vertical coordinate into pressure levels and then interpolating onto the air parcel's pressure in the vertical. In this way, we reconstruct the evolution of a variety of meteorological variables along the trajectory paths throughout the following analysis.

3. Results

Figures 1a and 1b show the trajectory paths for all samples (gray lines) from the coldest 5% (400 trajectories) and median

10% (1000 trajectories) of wintertime temperature anomalies in central North America. Cold air outbreaks generally travel out of the Arctic and southward or southeastward along the Rocky Mountains before arriving in the middle of the continent, whereas median-temperature events have a wider spread and travel more eastward off of the Pacific Ocean. However, not all Arctic air masses result in a cold air outbreak when advected into the midlatitudes; 76% of cold air outbreak trajectories spend time north of the Arctic Circle in the 10 days preceding the cold event, but 41% of median-temperature events do as well. This observation motivated us to subsample both cold air outbreak and median-temperature trajectories to distinguish which characteristics determine whether the arrival of an Arctic air mass results in a midlatitude cold-air outbreak. We selected 275 CAO and 262 MTE trajectories that all follow a similar path out of the Arctic to use throughout the rest of this study, shown in color in Fig. 1 (see section 2 for the selection method).

Subseasonal variations in climatology play a relatively minor role in the difference between our CAO and MTE. The distributions of cold air outbreaks and median-temperature events during the winter are shown in Fig. 2. Negative wintertime temperature anomalies over central North America, corresponding to cold air outbreaks as defined in our methodology, are somewhat more common in January, while the probability of median-temperature events is nearly constant across the winter months (colored dashed outlines). Our MTE sample (selected, as explained in section 2, to exclude travel over open ocean) shows greater seasonality than median-temperature events overall, as we see in Fig. 2b where the filled gold bars are less concentrated in late December and more in February than the dashed gold outline. The subseasonal variability in Fig. 2 implies that Arctic air masses traveling south in late December and January are relatively more likely to produce cold air outbreaks, while those traveling in February are more likely to produce median-temperature events. Rather than remove the subseasonal variation at the event identification step by subtracting the weekly mean instead of the seasonal mean, we
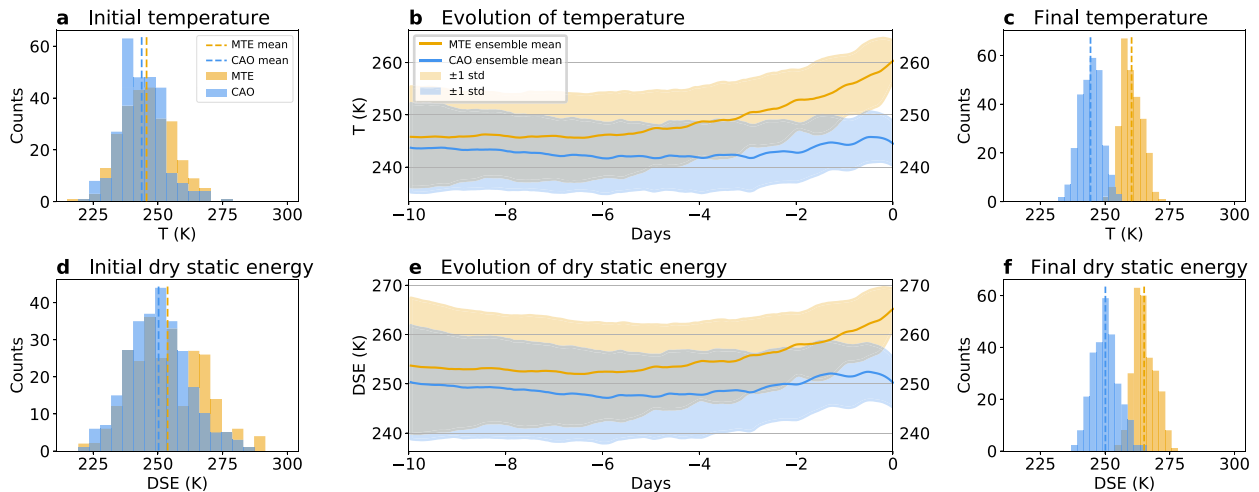
FIG. 3. (left) Initial distribution and (right) final distribution of (a),(c) temperature and (d),(f) DSE are shown for all CAO (blue) and MTE (gold) trajectories. (b),(e)Their evolution over each 10-day back trajectory, represented by the ensemble average (solid line) and one standard deviation (shading) across all trajectories for each case (275 CAO and 262 MTE). DSE is divided by specific heat c_p to give units of temperature. Given that CAO and MTE trajectories have similar DSE distributions 10 days before arriving in the midlatitudes, one concludes that the initial state alone does not determine whether an Arctic air mass becomes a cold air outbreak.

incorporate the subseasonal variability between CAO and MTE into our discussion of the differing physical mechanisms below.

Not all Arctic air masses result in cold air outbreaks, but is that a result of differences in initial temperature or in evolution along the trajectory? Figure 3a shows that initial temperature alone does not determine a cold air outbreak: CAOs and MTEs have a similar distribution of initial temperature 10 days before arriving in the midlatitudes (Fig. 3a), while the temperature evolution along each trajectory (Fig. 3b) demonstrates that CAO air masses (blue in the figure) generally cool over the first 6 days and then warm slightly for the final 4 days, while MTEs (gold) maintain temperature for 4 days and then warm. There are a handful of CAO trajectories with the same final temperature as MTEs (see overlap in histograms in Fig. 3c), which is both because the event sampling was based on 2-m temperature while the trajectories end at 100 m and because the DJF climatology varies across the sampling region such that a cold anomaly at one end may have the same temperature as a median anomaly at another. Dry static energy (DSE), which is conserved under adiabatic compression and expansion under the hydrostatic approximation, is also shown (Figs. 3d–f):

$$\text{DSE} = c_p T + gz, \qquad (1)$$

where T is temperature, g is gravitational acceleration, c_p is the specific heat of air, and z is geopotential height. When analyzing and showing dry static energy throughout this paper, it is divided by the specific heat of air c_p to give it units of temperature. While the initial DSE is 3 K warmer for MTEs on average (Fig. 3d), the difference on arrival in the sampling region is considerably larger (15 K; Fig. 3f). The divergence of DSE over time (Fig. 3e) indicates that adiabatic compression and expansion are not solely responsible

for the difference in temperature trends, and indeed the air parcel height above the ground has nearly the same distribution over time across CAO and MTE trajectories (not shown). Diabatic processes therefore must play a significant role in the temperature evolution of CAO and MTE air masses.

To study the causes of temperature and DSE changes along each trajectory, we investigate the temperature tendencies due to distinct physical processes. In CAM, the temperature rate of change at each grid point can be decomposed for each time step as

$$\dot{T} = \dot{T}_{\text{physics}} + \dot{T}_{\text{dynamics}} + \dot{T}_{\text{fix}}; \qquad (2)$$

$\dot{T}_{\text{dynamics}}$ is calculated by the dynamical core and accounts for advection, adiabatic compression and expansion, and the hopefully small divergence damping (Neale et al. 2012). The term $\dot{T}_{\text{fix}}$ is a very small energy correction that ensures the conservation of global energy. The model physics contribution $\dot{T}_{\text{physics}}$ can be further decomposed into distinct physical processes:

$$\dot{T}_{\text{physics}} = \text{M} + \text{SW} + \text{LW} + \text{VT} + \text{TTGWORO}, \qquad (3)$$

where the terms on the right are the temperature tendency due to moist processes (M), shortwave radiation (SW), longwave radiation (LW), vertical mixing (VT) (or vertical diffusion, which includes surface fluxes at the lower boundary), and gravity wave drag (TTGWORO).

In a Lagrangian frame following an air parcel trajectory, the dynamical component $\dot{T}_{\text{dynamics}}$ in Eq. (2) can be eliminated by using DSE [Eq. (1)] as the state variable instead of temperature. The change in DSE over a specified length of time along a Lagrangian air parcel trajectory can be decomposed into a direct sum of diabatic temperature tendencies:

$$\dot{\text{DSE}} = \text{M} + \text{SW} + \text{LW} + \text{VT} + \text{TTGWORO} + \dot{T}_{\text{fix}}$$
$$\approx \text{M} + \text{SW} + \text{LW} + \text{VT}, \quad \text{or}$$
$$\Delta\text{DSE} \approx \int (\text{M} + \text{SW} + \text{LW} + \text{VT}) \, dt$$
$$= \int \dot{T}_{\text{physics}} \, dt, \tag{4}$$

where the second line and beyond drop TTGWORO and $\dot{T}_{\text{fix}}$, both of which are at least two orders of magnitude smaller than all other terms in the region of interest. Equation (4) represents a DSE budget in the Lagrangian frame, where the left-hand side is the change in instantaneous DSE over a given time period, and the right-hand side is the integral of the average temperature tendency over that same time period. In line with this convention, plots and analysis of DSE throughout this paper use instantaneous values, while those of temperature tendencies and all other variables use hourly averages. We can interpolate each of the temperature tendency terms on the right-hand side onto trajectory paths calculated by HYSPLIT to get the contribution of each physical process to the change in DSE along that trajectory.

The contributions of distinct diabatic processes to DSE change along Arctic air parcel trajectories are shown by the blue CAO and gold MTE curves in Fig. 4. The integrated total physics temperature tendency $\int \dot{T}_{\text{physics}} \, dt$ (Fig. 4b) demonstrates that CAO air masses undergo more diabatic cooling than their MTE counterparts, for a total of −10 K versus +6 K over the 10-day trajectories on average. As the DSE 10 days before arrival in the midlatitudes was roughly 3 K cooler for CAOs (recall the initial DSE distributions in Fig. 3d), the additional diabatic cooling of −16 K would result in a DSE difference between CAOs and MTEs on arrival of just under 20 K. One would expect, given Eq. (4), that the integrated total temperature tendency (right-hand side) is equal to the total change in DSE (left-hand side) along a trajectory. However, the difference in total temperature tendency between CAO and MTE is about 20 K, while the difference in DSE change is 15 K. This mismatch is due to budget closure errors (Fig. 3l) that will be discussed later in this section.

The physical process that dominates the difference in total temperature tendency over 10-day trajectories between CAO and MTE is vertical mixing VT. The vertical mixing tendency, integrated over a 10-day trajectory, is −3.5 ± 11 K on average for CAOs versus +13.5 ± 13 K for MTEs, giving a 17-K difference between CAOs and MTEs. The histograms of the total contribution of VT have the least overlap of any temperature tendency component (Fig. 4d). This is also reflected in the fact that the blue CAO curve is below the gold MTE curve most of the time in Fig. 4c. Tendencies due to longwave radiation LW are on the order of −10 K over each trajectory, but both CAO and MTE trajectories experience a similar magnitude of longwave cooling (Fig. 4f). The contributions of latent heating (moist processes M) and shortwave absorption by the air parcel SW are negligible (on the order of 1 K in Figs. 4h,j).

As LW and VT are the largest contributions to $\dot{T}_{\text{physics}}$, it is worth discussing their behavior in more detail. LW is small in magnitude on an hourly basis, which we can see by comparing hourly LW evolution in Fig. 4e to the total physics tendency in Fig. 4a. But the LW contribution is consistent over the entire trajectory path, such that the integrated LW contribution (Fig. 4f) is a significant component of $\int \dot{T}_{\text{physics}} \, dt$ (Fig. 4b). By contrast, VT along individual trajectories is usually zero, with infrequent but high-magnitude excursions into strong cooling or warming. The episodic behavior of VT is evident in the larger standard deviation relative to LW in Figs. 4c and 4e, as the average standard deviation along a trajectory is on the order of 0.5 K h^{-1} for VT versus 0.05 K h^{-1} for LW. The large standard deviation for VT indicates that a relatively small number of intense vertical mixing episodes may be an important factor in determining whether or not an Arctic air mass becomes a cold air outbreak. We also note that the relatively coarse vertical resolution of the model near the surface (50–100 m) may affect the relative contribution of vertical mixing. Repeating this analysis with a higher-resolution model would increase confidence in these results.

To understand the role of vertical mixing temperature tendency VT, we note that it contains contributions due to vertical eddy diffusion with a diffusion coefficient K_H, a nonlocal mixing term γ_H, heating due to kinetic energy dissipation D, and surface sensible heat flux (SHF), which is incorporated into VT only at the lowest model level. Of these, the sensible heat flux shows the most significant difference between CAO and MTE. To demonstrate its impact on vertical mixing VT, Fig. 5 shows the surface sensible heat flux after masking to return zero when the corresponding trajectory height is above 100 m, isolating the region sufficiently close to the surface for the sensible heat flux to contribute to the vertical mixing tendency (VT).

We cannot entirely rule out significant contributions due to eddy diffusivity K_H and nonlocal mixing γ_H, as computational limitations and available model diagnostics prevented us from retrieving these variables over the 51 years under study here. However, based on a detailed analysis of one winter of model output (not shown), we found that the eddy diffusivity K_H and nonlocal mixing γ_H tend to be much smaller in magnitude when VT < 0 than when VT > 0, so they are unlikely to be responsible for the cooling along CAO trajectories.

The above discussion of the sensible heat flux suggests that the surface energy balance under the moving air parcels can lead to additional insights into the conditions affecting Arctic airmass transformation. Figure 6 shows the terms of the surface energy balance. The downwelling longwave flux holds approximately constant along CAO trajectories but rises steadily along MTE trajectories and then rises abruptly on the final day (Fig. 6c). The upwelling longwave flux exhibits similar behavior (Fig. 6e), consistent with a cold surface underlying CAOs and a warmer surface for MTEs (Fig. 6i). The net solar flux is slightly higher on average for MTEs (Fig. 6h), corresponding to more heat absorption by the surface. Some of the differences in net solar flux could result from subseasonal variability, as MTEs are relatively more likely to occur in February (Fig. 2) when the polar night is shorter. All of the terms affecting the surface energy budget contribute to a colder surface underlying CAO trajectories than MTE trajectories
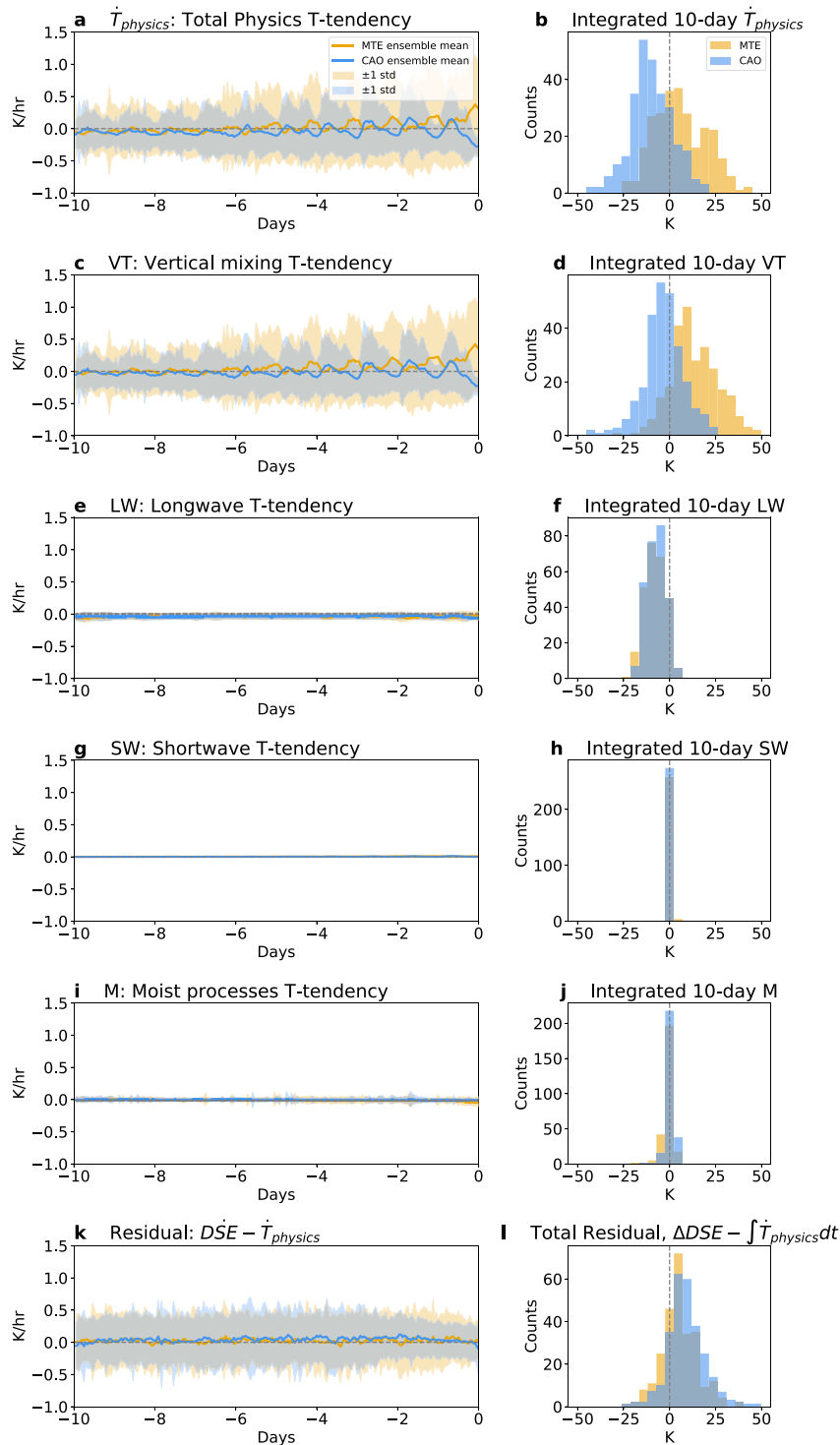
FIG. 4. (a) The evolution of total physics temperature tendency and (c),(e),(g),(i) each of its four major components, with (b),(d),(f),(h),(j) histograms of the integral of each tendency over each trajectory. (k) The hourly budget closure residual (DSE − $\dot{T}_{\text{physics}}$) and (l) the total budget closure residual over all 10 days (ΔDSE − $\int \dot{T}_{\text{physics}} \, dt$). The total physics temperature tendency in (b) demonstrates that, on average, CAO air masses cool on the order of −10 K while MTEs warm by +6 K. Vertical mixing in (d) dominates the difference in diabatic heating and cooling between CAO and MTE trajectories.
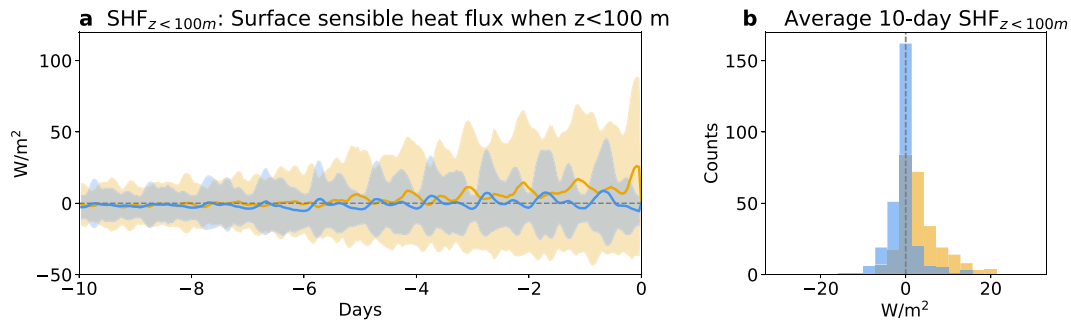
FIG. 5. Surface sensible heat flux, masked to only include values when the trajectory height is less than 100 m and to return zero otherwise, roughly corresponding to heights at which the sensible heat flux contributes to vertical mixing temperature tendency (VT). (a) The ensemble average across all trajectories (solid line) plus and minus one standard deviation (shaded region) in blue for CAO and gold for MTE trajectories. (b) The distribution across the CAO and MTE cases of the average value along each trajectory. The dashed gray lines correspond to zero.

(expressed by the 2-m temperature in Figs. 6i,j), consistent with the role of cooling by sensible heat flux demonstrated in Fig. 5.

It is important to quantify the uncertainty in the above interpretation of the temperature tendency components. The DSE budget should, by breaking down the change in DSE into the temperature tendency from each physical process in the model, allow for the direct attribution of temperature changes to mechanisms like latent heating and longwave radiative cooling. Previous studies using Lagrangian trajectories have generally looked at the change in potential temperature alone and from that deduced (by conjunction with specific humidity or surface fluxes) or speculated the physical processes responsible (Papritz et al. 2015; Papritz and Spengler 2017; Zschenderlein et al. 2019; Hermann et al. 2020). However, because we attempt a more detailed analysis by explicitly calculating each component of diabatic temperature change and comparing it to the change in DSE, we find that the DSE budget along individual trajectories does not close exactly. That is, the integral of the total diabatic temperature tendency over a trajectory $\int \dot{T}_{\text{physics}} \, dt$ is generally not exactly equal to the total DSE change along the trajectory ΔDSE, as shown in Fig. 4l. This is most likely the result of imperfect trajectory calculations due to the necessary discretization of space and time. The budget closure difficulties may result from advection errors in CAM that lead to implicit artificial mixing due to the discretization of the advection terms (Durran 2010). Such mixing would affect the time rate of change in the Eulerian model but would not lead to budget closure problems there. However, in a Lagrangian framework, where the advection is replaced by a trajectory calculation, the artificial mixing is not present, leading to budget closure problems. Another source of difficulties may be interpolation errors in HYSPLIT in the presence of strong vertical temperature gradients, where small errors in the vertical location can lead to large changes in DSE even in the absence of diabatic forcing. We found the budget closure error to be negligible when applying our methodology in a midlatitude region with no surface inversions (not shown), whereas the CAO and MTE trajectories analyzed here frequently experience strong surface temperature

inversions ($d\text{DSE}/dz > 0$ at most times along almost all CAO and MTE trajectories, not shown). The above challenges with trajectory calculation mean that relying solely on DSE changes along a trajectory to diagnose diabatic temperature changes is not necessarily more reliable than using the temperature tendencies output by the model, hence our decision to use both.

The departure from budget closure accumulated across all 10 days of each trajectory, shown in Fig. 4l as $\Delta\text{DSE} - \int \dot{T}_{\text{physics}} \, dt$, is $+9.5 \pm 11$ K for CAOs and $+5.6 \pm 10$ K for MTEs, which in some cases is on the order of the total change in DSE. There is a systematic element to this error, as the total change in DSE tends to be greater than the total physics temperature tendency (average residual > 0 in Fig. 4l). Focusing on the difference between CAOs and MTEs eliminates some of the systematic error. The total change in DSE along the 10-day trajectory is 11.6 K more negative on average for CAOs than for MTEs (16-K difference in total temperature tendency), which is greater than the difference in the budget closure error. This bolsters our confidence in the results, especially given the fairly large sample sizes (>250 in each case) and the separation of the distributions of integrated diabatic temperature tendencies $\int \dot{T}_{\text{physics}} \, dt$ between CAO and MTE trajectories (Fig. 4b). Overall, while our attempt to calculate a budget for traveling air parcels is potentially an improvement over previous studies that assumed all changes in DSE represent diabatic temperature effects, our budget closure errors indicate that this approach needs to be further improved.

Large-scale dynamics also play an interesting role, as seen in Fig. 7. We constructed composites across all CAO and all MTE events of the sea level pressure and total cloud fraction fields on the day the events were identified, then subtracted MTE from CAO to display the difference between the two cases. The strongest signal is over the sampling region itself, where the CAO composite has a sea level pressure almost 15 hPa higher than the MTE case, shown in Fig. 7a. The sea level pressure anomaly composites for CAO and MTE individually (not shown) confirm that the difference between CAO and MTE is driven by a positive anomaly during CAOs
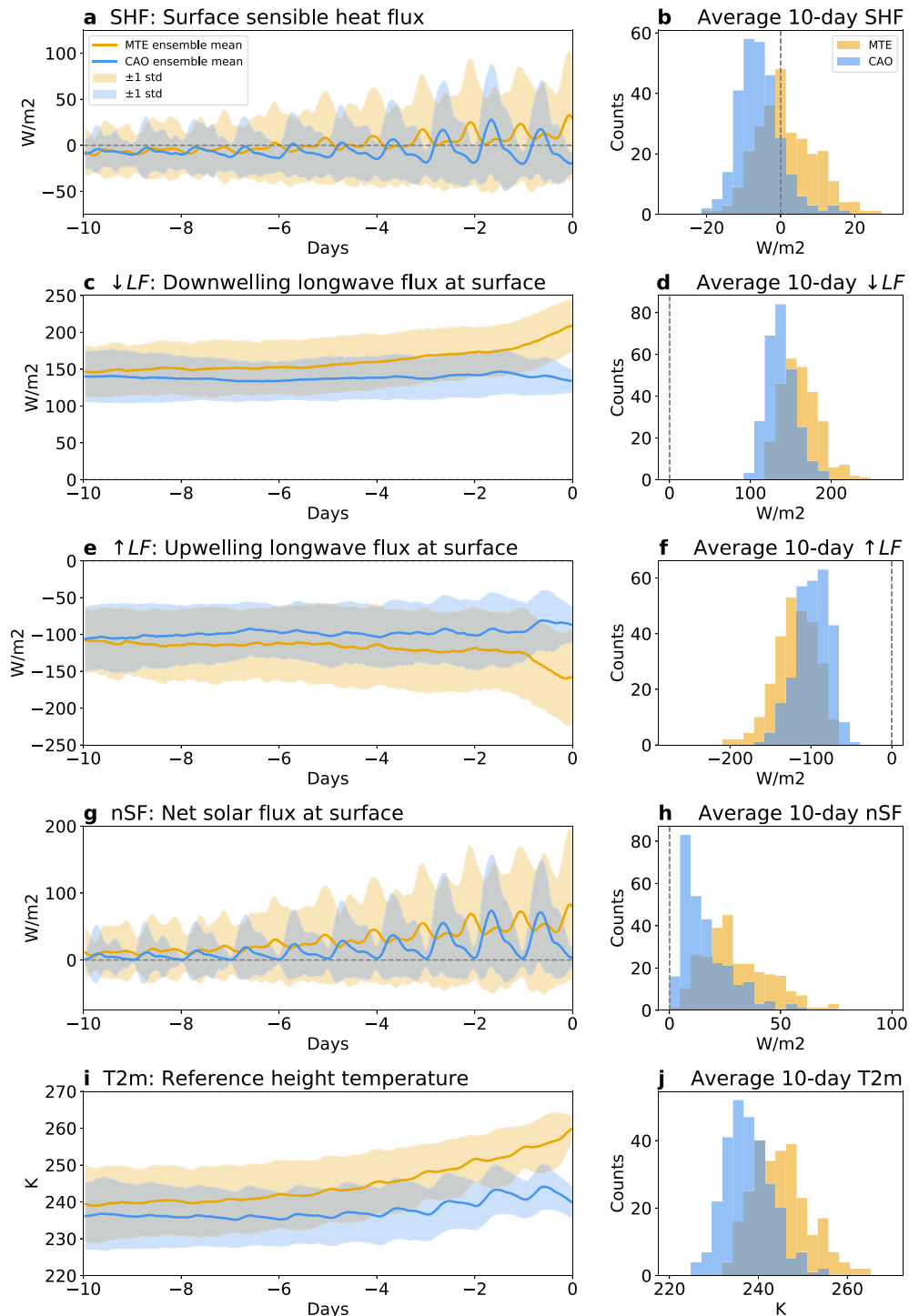
FIG. 6. Surface energy fluxes underlying trajectories are shown, with (a),(c),(e),(g) their evolution as a function of time and (b),(d),(f),(h) the distribution of average values . The evolution plots show the ensemble average across all trajectories (solid line) plus and minus one standard deviation (shaded region) in blue for CAO and gold for MTE trajectories. The histograms show the distribution across the CAO and MTE cases of the average value along each trajectory. (i),(j) The 2-m temperature underlying each trajectory as a proxy for the surface temperature to assist in interpretation. The dashed gray lines correspond to zero, while positive values indicate downward energy flux and negative values indicate upward [except for sensible heat flux in (a) and (b), where positive values correspond to warming of near-surface air and negative to cooling].

Difference in Composite Sea Level Pressure,
CAO - MTE, on Day of Event

Difference in Composite Vertically-integrated Cloud Fraction,
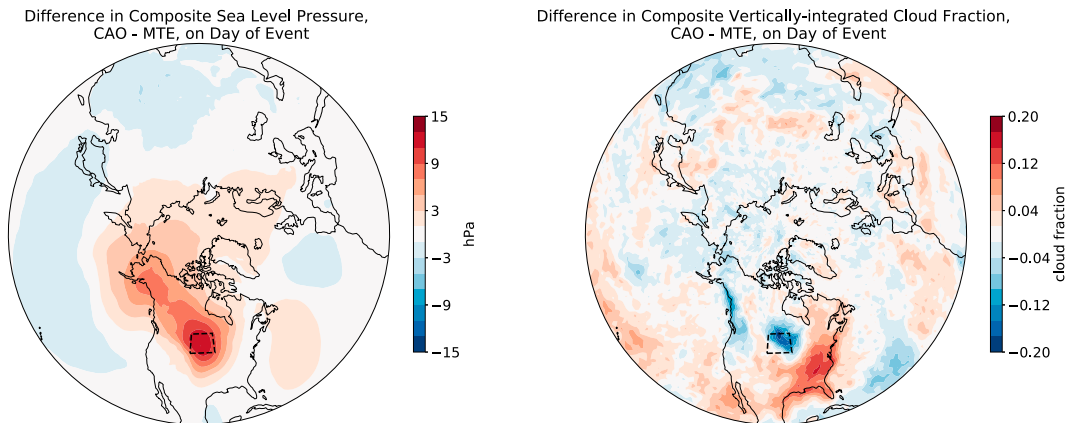CAO - MTE, on Day of Event

FIG. 7. The difference, calculated as CAO minus MTE, in composites of (left) sea level pressure and (right) vertically integrated total cloud fraction. Each composite is an average over all events in the corresponding study sample (275 for CAO, 262 for MTE) of the meteorological field at the time the event was identified within the sampling region (black dashed box).

rather than a negative anomaly during MTE. A higher sea level pressure is consistent with more subsidence during CAOs than MTEs, which is reflected in the corresponding decrease in cloud cover in Fig. 7b. The difference in cloud cover is driven by a decrease in both low- and midlevel clouds for CAO (not shown). While subsidence is usually also associated with warming, these air parcels are already close to the ground (recall that the back trajectories are initiated at 100 m on day 0), so large-scale subsidence acts primarily to clear cloud cover and keep downwelling longwave fluxes low in the final day of CAOs. The effect on the downwelling longwave flux ($\downarrow$LF) is evident in Fig. 6c, where $\downarrow$LF continues to rise for MTE in the final day but levels off for CAO. In principle, sea level pressure could direct trajectories along different paths for CAOs versus MTEs. However, given that the trajectory paths for CAOs and MTEs are similar by construction (Fig. 1) and the air parcel heights do not noticeably differ (see discussion of Fig. 3), we do not expect the large-scale dynamics to be different preceding the two cases. On the other hand, large-scale dynamics could contribute to the preconditioning that establishes surface temperature differences underlying CAOs and MTEs (see discussion of Fig. 6).

4. Conclusions

Wintertime cold air outbreaks are periods of extreme cold, often persisting for several days and spanning hundreds of kilometers or more, that are commonly associated with intrusions of cold polar air into the midlatitudes (Walsh et al. 2001; Cellitti et al. 2006; Portis et al. 2006; Vavrus et al. 2006; Kolstad et al. 2010; Hankes and Walsh 2011; Smith and Sheridan 2018). Despite a clear warming signal in average temperatures, there is a lack of consensus in the literature on whether continental cold air outbreaks have declined over the past several decades (Walsh et al. 2001; Portis et al. 2006; Hankes and Walsh 2011; Liu et al. 2012; Westby et al. 2013; Cohen et al. 2014; Robeson et al. 2014; Screen 2014; van Oldenborgh et al. 2019; Smith and Sheridan 2020), indicating that there

may be some mechanism to maintain them in spite of the overall warming trend.

In this work, we set out to examine the relative importance of the initial temperature of an air mass originating in the Arctic versus diabatic warming and cooling of the air mass on its way into the midlatitudes to result in a cold air outbreak over North America. We study the processes affecting air parcels traveling over sea ice and land on their way to causing cold air outbreaks by comparing them to those that follow a similar path but result in median temperatures upon arrival in the midlatitudes.

Previous studies of cold air outbreak origins identified the Arctic as an important source region and then implicitly assumed that cold initial temperatures would lead to cold air outbreaks when advected into the midlatitudes (Kalkstein et al. 1990; Walsh et al. 2001; Hankes and Walsh 2011). However, we find that there is significant overlap in the initial dry static energy distributions of wintertime Arctic air masses leading to CAOs versus those leading to MTEs upon arrival in the midlatitudes. Diabatic processes, therefore, must play a significant role in the development of cold air outbreaks.

We consider temperature tendencies from distinct diabatic processes along each trajectory to determine the mechanisms controlling diabatic temperature evolution. We find that longwave radiative cooling and vertical mixing are the two dominant contributors to temperature evolution along both CAO and MTE trajectories, whereas shortwave radiative heating of the air parcel and latent heating are negligible. However, it is vertical mixing that sets cold air outbreaks apart from median-temperature events, causing, on average, 17 K more cooling over 10 days for CAO versus MTE trajectories. Examining the contributions to the vertical mixing term, we find that the surface sensible heat flux generally cools CAO air parcels as they travel near the lowest model level but warms MTEs. The cooling of CAOs due to sensible heat flux is consistent with the colder surface and smaller net surface shortwave radiation we find to be underlying these trajectories.

Seasonality plays some role, as Arctic air masses are more likely to develop into CAOs in midwinter, while MTEs are relatively more likely in February when the days are longer. However, given that the initial temperature distributions for CAOs and MTEs are nearly the same, the seasonality is expressed primarily through differences in the net surface shortwave flux that support a colder or warmer underlying surface along the path of travel into the midlatitudes. Subsidence over the cold air outbreak region on the final day can also, perhaps counterintuitively, help to maintain cold temperatures near the surface. Subsidence results in adiabatic warming, leading to drying of the mid- and lower troposphere that clears out low and midlevel clouds, allowing longwave radiation from the surface to escape to space.

In summary, our results suggest that cold air outbreaks resulting from Arctic air masses require strong cooling from surface sensible heat fluxes during their journey into the midlatitudes. Diabatic cooling from longwave radiation is reinforced by these sensible heat fluxes and the redistribution of the cooled surface air up into the air column by vertical mixing.

Our results are confined to a preindustrial climate scenario, but based on the mechanisms identified, we can speculate on how cold air outbreak development might change in a warmer climate. Surface sensible heat fluxes appear to be key in cooling Arctic air masses. Temperature contrasts between low-lying air and the underlying surface drive sensible heat fluxes, implying a role for preconditioning of the surface. We identified differences in the net solar flux at the surface (Fig. 6h) as a possible contributor to differences in sensible heat flux and surface temperature for CAOs and MTEs (Figs. 5 and 6b). As sea ice retreats and the Arctic Ocean is exposed in a warming climate, air masses are likely to encounter more upward turbulent heat fluxes from the ocean in the Arctic. Decreases to surface albedo as snow cover retreats earlier in the winter will likely also contribute to a warmer land surface and more positive sensible heat flux, potentially inhibiting the development of Arctic cold air outbreaks. But sea ice in the Arctic and snow cover in high-latitude North America are subject to large regional and temporal variability (Cavalieri and Parkinson 2012; Mudryk et al. 2020), and snow cover in particular does not necessarily decrease consistently with warming (Brown 2000). This sensitivity may help explain the regional and temporal variability of cold air outbreak trends that is demonstrated by the lack of consensus regarding a global warming signal in observations (Walsh et al. 2001; Portis et al. 2006; Hankes and Walsh 2011; Liu et al. 2012; Westby et al. 2013; Cohen et al. 2014; Robeson et al. 2014; Screen 2014; van Oldenborgh et al. 2019; Smith and Sheridan 2020) and by disagreement across CMIP models (Vavrus et al. 2006).

There are a few caveats to the applicability of our results that are important to keep in mind. The main quantitative limitation is in the lack of closure of the dry static energy budget, discussed in section 3. The budget error along individual trajectories (change in DSE along the trajectory is not exactly equal to the sum of all time-integrated diabatic temperature tendencies) can be large. However, focusing as we do on the difference between the two populations of CAO and MTE trajectories still reveals significant differences in vertical mixing and sensible heat flux, which are the dominant players in our proposed mechanism for the difference between CAO and MTE events. Regardless of such errors, our approach still represents a more detailed analysis than was possible in previous studies, which combined all diabatic processes into a single diabatic tendency term as mentioned in the introduction; we find that longwave radiation and vertical mixing are significant contributors to temperature change, while latent heating and shortwave radiative heating of the air parcel have little effect. We also note that the relatively coarse vertical resolution of the model near the surface may affect the relative contribution of vertical mixing. The other main limitation of our study is by design, as we chose to focus specifically on air masses that are Arctic in origin and share a similar path of travel into a specific region within North America. Our results, therefore, may not generalize to all cold air outbreaks, as they represent a narrow subset of source regions and paths of travel. We made this choice to focus on the subset of trajectories that originate in the Arctic, as these are most representative of the typical path of travel for continental cold air outbreaks (Walsh et al. 2001; Hankes and Walsh 2011). Focusing on such air masses of Arctic origin also helps us isolate the relative influence of origin versus evolution on the eventual midlatitude temperature, which in turn constrains our ability to generalize.

Data availability statement. Simulations were performed using CESM1.2.2 with CAM5, which is freely available at http://www.cesm.ucar.edu/models/cesm1.2/ following registration. Back trajectories were calculated using HYSPLIT v5.1.0 (with modifications described in section 2), which is freely available at https://www.ready.noaa.gov/HYSPLIT.php. Code used to interpolate CAM data onto HYSPLIT trajectories is available on GitHub at https://github.com/kahartig/camtrack.

REFERENCES

André, J. C., and L. Mahrt, 1982: The nocturnal surface inversion and influence of clear-air radiative cooling. *J. Atmos. Sci.*, **39**, 864–878, https://doi.org/10.1175/1520-0469(1982)039<0864:TNSIAI>2.0.CO;2.

Arias, P. A., and Coauthors, 2021: Technical summary. *Climate Change 2021: The Physical Science Basis*, V. Masson-Delmotte et al., Eds., Cambridge University Press, 33–144, https://www.ipcc.ch/report/ar6/wg1/downloads/report/IPCC_AR6_WGI_TS.pdf.

Bieli, M., S. Pfahl, and H. Wernli, 2015: A Lagrangian investigation of hot and cold temperature extremes in Europe. *Quart. J. Roy. Meteor. Soc.*, **141**, 98–108, https://doi.org/10.1002/qj.2339.

Brown, R. D., 2000: Northern Hemisphere snow cover variability and change, 1915–97. *J. Climate*, **13**, 2339–2355, https://doi.org/10.1175/1520-0442(2000)013<2339:NHSCVA>2.0.CO;2.

Cavalieri, D. J., and C. L. Parkinson, 2012: Arctic sea ice variability and trends, 1979–2010. *Cryosphere*, **6**, 881–889, https://doi.org/10.5194/tc-6-881-2012.

Cellitti, M. P., J. E. Walsh, R. M. Rauber, and D. H. Portis, 2006: Extreme cold air outbreaks over the United States, the polar vortex, and the large-scale circulation. *J. Geophys. Res.*, **111**, D02114, https://doi.org/10.1029/2005JD006273.

Cohen, J., and Coauthors, 2014: Recent Arctic amplification and extreme mid-latitude weather. *Nat. Geosci.*, **7**, 627–637, https://doi.org/10.1038/ngeo2234.

Cronin, T. W., and E. Tziperman, 2015: Low clouds suppress Arctic air formation and amplify high-latitude continental winter warming. *Proc. Natl. Acad. Sci. USA*, **112**, 11 490–11 495, https://doi.org/10.1073/pnas.1510937112.

Curry, J., 1983: On the formation of continental polar air. *J. Atmos. Sci.*, **40**, 2278–2292, https://doi.org/10.1175/1520-0469(1983)040<2278:OTFOCP>2.0.CO;2.

Dee, D. P., and Coauthors, 2011: The ERA-Interim reanalysis: Configuration and performance of the data assimilation system. *Quart. J. Roy. Meteor. Soc.*, **137**, 553–597, https://doi.org/10.1002/qj.828.

Draxler, R. R., 1999: HYSPLIT 4 user's guide. NOAA Tech. Rep. ERL ARL-230, 38 pp.

——, and G. D. Hess, 1997: Description of the HYSPLIT_4 modeling system. NOAA Tech. Memo. ERL ARL-224, 24 pp., https://www.arl.noaa.gov/documents/reports/arl-224.pdf.

——, and ——, 1998: An overview of the HYSPLIT_4 modelling system for trajectories, dispersion, and deposition. *Aust. Meteor. Mag.*, **47**, 295–308.

Durran, D. R., 2010: Finite-difference approximations for one-dimensional transport. *Numerical Methods for Fluid Dynamics: With Applications to Geophysics*, D. R. Durran, Ed., Springer, 89–146, https://doi.org/10.1007/978-1-4419-6412-0_3.

Gao, Y., L. R. Leung, J. Lu, and G. Masato, 2015: Persistent cold air outbreaks over North America in a warming climate. *Environ. Res. Lett.*, **10**, 044001, https://doi.org/10.1088/1748-9326/10/4/044001.

Gerber, E. P., and Coauthors, 2012: Assessing and understanding the impact of stratospheric dynamics and variability on the Earth system. *Bull. Amer. Meteor. Soc.*, **93**, 845–859, https://doi.org/10.1175/BAMS-D-11-00145.1.

Hankes, I. E., and J. E. Walsh, 2011: Characteristics of extreme cold air masses over the North American sub-Arctic. *J. Geophys. Res.*, **116**, D11102, https://doi.org/10.1029/2009JD013582.

Hermann, M., L. Papritz, and H. Wernli, 2020: A Lagrangian analysis of the dynamical and thermodynamic drivers of large-scale Greenland melt events during 1979–2017. *Wea. Climate Dyn.*, **1**, 497–518, https://doi.org/10.5194/wcd-1-497-2020.

Hitchcock, P., and I. R. Simpson, 2014: The downward influence of stratospheric sudden warmings. *J. Atmos. Sci.*, **71**, 3856–3876, https://doi.org/10.1175/JAS-D-14-0012.1.

Hurrell, J. W., Y. Kushnir, G. Ottersen, and M. Visbeck, 2003: An overview of the North Atlantic Oscillation. *The North Atlantic Oscillation: Climatic Significance and Environmental Impact*, Geophys. Monogr., Vol. 134, Amer. Geophys. Union, 1–35, https://doi.org/10.1029/134GM01.

——, and Coauthors, 2013: The Community Earth System Model: A framework for collaborative research. *Bull. Amer. Meteor. Soc.*, **94**, 1339–1360, https://doi.org/10.1175/BAMS-D-12-00121.1.

Kalkstein, L. S., P. C. Dunne, and R. S. Vose, 1990: Detection of climatic change in the western North American Arctic using a synoptic climatological approach. *J. Climate*, **3**, 1153–1167, https://doi.org/10.1175/1520-0442(1990)003<1153:DOCCIT>2.0.CO;2.

Kidston, J., A. A. Scaife, S. C. Hardiman, D. M. Mitchell, N. Butchart, M. P. Baldwin, and L. J. Gray, 2015: Stratospheric influence on tropospheric jet streams, storm tracks and surface weather. *Nat. Geosci.*, **8**, 433–440, https://doi.org/10.1038/ngeo2424.

Kolstad, E. W., T. Breiteig, and A. A. Scaife, 2010: The association between stratospheric weak polar vortex events and cold air outbreaks in the Northern Hemisphere. *Quart. J. Roy. Meteor. Soc.*, **136**, 886–893, https://doi.org/10.1002/qj.620.

Konrad, C. E., and S. J. Colucci, 1989: An examination of extreme cold air outbreaks over eastern North America. *Mon. Wea. Rev.*, **117**, 2687–2700, https://doi.org/10.1175/1520-0493(1989)117<2687:AEOECA>2.0.CO;2.

Liu, J., J. A. Curry, H. Wang, M. Song, and R. M. Horton, 2012: Impact of declining Arctic sea ice on winter snowfall. *Proc. Nat. Acad. Sci. USA*, **109**, 4074–4079, https://doi.org/10.1073/pnas.1114910109.

Mudryk, L., M. Santolaria-Otín, G. Krinner, M. Ménégoz, C. Derksen, C. Brutel-Vuilmet, M. Brady, and R. Essery, 2020: Historical Northern Hemisphere snow cover trends and projected changes in the CMIP6 multi-model ensemble. *Cryosphere*, **14**, 2495–2514, https://doi.org/10.5194/tc-14-2495-2020.

Neale, R. B., and Coauthors, 2012: Description of the NCAR Community Atmosphere Model (CAM 5.0). NCAR Tech. Note NCAR/TN-4861STR, National Center for Atmospheric Research, 289 pp.

NOAA/ARL, 2022: HYSPLIT user's guide. Accessed 1 January 2022, https://www.ready.noaa.gov/hysplitusersguide/index.htm.

Papritz, L., and T. Spengler, 2017: A Lagrangian climatology of wintertime cold air outbreaks in the Irminger and Nordic seas and their role in shaping air–sea heat fluxes. *J. Climate*, **30**, 2717–2737, https://doi.org/10.1175/JCLI-D-16-0605.1.

——, S. Pfahl, H. Sodemann, and H. Wernli, 2015: A climatology of cold air outbreaks and their impact on air–sea heat fluxes in the high-latitude South Pacific. *J. Climate*, **28**, 342–364, https://doi.org/10.1175/JCLI-D-14-00482.1.

Portis, D. H., M. P. Cellitti, W. L. Chapman, and J. E. Walsh, 2006: Low-frequency variability and evolution of North American cold air outbreaks. *Mon. Wea. Rev.*, **134**, 579–597, https://doi.org/10.1175/MWR3083.1.

Quiroz, R. S., 1984: The climate of the 1983–84 winter—A season of strong blocking and severe cold in North America. *Mon. Wea. Rev.*, **112**, 1894–1912, https://doi.org/10.1175/1520-0493(1984)112<1894:TCOTWS>2.0.CO;2.

Robeson, S. M., C. J. Willmott, and P. D. Jones, 2014: Trends in hemispheric warm and cold anomalies. *Geophys. Res. Lett.*, **41**, 9065–9071, https://doi.org/10.1002/2014GL062323.

Rogers, J. C., and R. V. Rohli, 1991: Florida citrus freezes and polar anticyclones in the Great Plains. *J. Climate*, **4**, 1103–1113, https://doi.org/10.1175/1520-0442(1991)004<1103:FCFAPA>2.0.CO;2.

Screen, J. A., 2014: Arctic amplification decreases temperature variance in northern mid- to high-latitudes. *Nat. Climate Change*, **4**, 577–582, https://doi.org/10.1038/nclimate2268.

Smith, E. T., and S. C. Sheridan, 2018: The characteristics of extreme cold events and cold air outbreaks in the eastern United States. *Int. J. Climatol.*, **38**, e807–e820, https://doi.org/10.1002/joc.5408.

——, and ——, 2019: The influence of extreme cold events on mortality in the United States. *Sci. Total Environ.*, **647**, 342–351, https://doi.org/10.1016/j.scitotenv.2018.07.466.

——, and ——, 2020: Where do cold air outbreaks occur, and how have they changed over time? *Geophys. Res. Lett.*, **47**, e2020GL086983, https://doi.org/10.1029/2020GL086983.

Stein, A. F., R. R. Draxler, G. D. Rolph, B. J. B. Stunder, M. D. Cohen, and F. Ngan, 2015: NOAA's HYSPLIT Atmospheric Transport and Dispersion Modeling System. *Bull. Amer. Meteor. Soc.*, **96**, 2059–2077, https://doi.org/10.1175/BAMS-D-14-00110.1.

Thompson, D. W. J., and J. M. Wallace, 2001: Regional climate impacts of the Northern Hemisphere annular mode. *Science*, **293**, 85–89, https://doi.org/10.1126/science.1058958.

van Oldenborgh, G. J., E. Mitchell-Larson, G. A. Vecchi, H. de Vries, R. Vautard, and F. Otto, 2019: Cold waves are getting milder in the northern midlatitudes. *Environ. Res. Lett.*, **14**, 114004, https://doi.org/10.1088/1748-9326/ab4867.

Vavrus, S., J. E. Walsh, W. L. Chapman, and D. Portis, 2006: The behavior of extreme cold air outbreaks under greenhouse warming. *Int. J. Climatol.*, **26**, 1133–1147, https://doi.org/10.1002/joc.1301.

Walsh, J. E., A. S. Phillips, D. H. Portis, and W. L. Chapman, 2001: Extreme cold outbreaks in the United States and Europe, 1948–99. *J. Climate*, **14**, 2642–2658, https://doi.org/10.1175/1520-0442(2001)014<2642:ECOITU>2.0.CO;2.

Wang, F., S. J. Vavrus, J. A. Francis, and J. E. Martin, 2019: The role of horizontal thermal advection in regulating wintertime mean and extreme temperatures over interior North America during the past and future. *Climate Dyn.*, **53**, 6125–6144, https://doi.org/10.1007/s00382-019-04917-8.

Westby, R. M., Y.-Y. Lee, and R. X. Black, 2013: Anomalous temperature regimes during the cool season: Long-term trends, low-frequency mode modulation, and representation in CMIP5 simulations. *J. Climate*, **26**, 9061–9076, https://doi.org/10.1175/JCLI-D-13-00003.1.

Zschenderlein, P., A. H. Fink, S. Pfahl, and H. Wernli, 2019: Processes determining heat waves across different European climates. *Quart. J. Roy. Meteor. Soc.*, **145**, 2973–2989, https://doi.org/10.1002/qj.3599.